Introduction of an organic acid phase changing material into metal-organic frameworks and the study of its thermal properties.

Yi Luan, Ming Yang, Qianqian Ma, Yue Qi, Hongyi Gao, Zhenyu Wu and Ge Wang*

School of Materials Science and Engineering, University of Science and Technology Beijing, Beijing 100083, P. R. China Fax: +86 10 62327878; Tel: +86 10 62333765; E-mail: gewang@mater.ustb.edu.cn

Supporting Information

Table of Contents

General Information. The structure and phase of the samples were evaluated by X-ray powder diffraction (XRD, Rigaku DMAX-RB 12 KW) with Cu Kα radiation (λ=0.15406 nm). The morphology of the as-obtained product was characterized by scanning electron microscopy (SEM, ZEISS SUPRA55). The samples for the SEM, TEM and HRTEM measurements were dispersed in ethanol and sonicated for a few minutes and supported onto the silicon slice and the holey carbon film on a Cu grid, respectively. The specific surface areas were calculated by the Brunauer–Emmett–Teller (BET) method. The pore size distributions were derived from the adsorption branches of isotherms by using the Barrett–Joyner–Halenda (BJH) model. Fourier transform Infrared spectra (FT-IR) were acquired on a Nicolet 6700 using the potassium bromide (KBr) pellet technique. Surface morphology and structure were observed by field emission scanning electron microscope on a SUPRA 55 (ZEISS, German) instrument operating at an accelerated voltage of 20 kV. The surface of the samples was sprayed with carbon. X-ray diffraction was measured with a Rigaku D_{MAX}-RB rotating anode diffractometer using Cu-Kα radiation (λ=1.5406 Å) at 40 kV and 150 mA. Diffraction patterns were collected in the 2θ ranges from 10° to 100°. Thermal properties of the fatty acid@MOF composite phase change materials were characterized by differential scanning calorimetry (DSC) using a NETZSCH STA449F3 (Germany) at a heating rate of 10 °C/min as well as a cooling rate of 10 °C/min. Samples (7±1 mg) were measured into Al_2O_3 pans with covers. The instrument was calibrated with reference to the enthalpy and melting point of indium (melting temperature: 429.6 K; ΔH_f : 28.6 J/g) , bismuth (melting temperature: 544.4 K; ΔH_f : 53.1 J/g) , zinc (melting temperature: 692.5 K; ΔH_f : 107.5 J/g), aluminum (melting temperature: 933.3 K; ΔH_f : 397 J/g) and gold (melting temperature: 1337.2 K; ΔH_f : 63.7 J/g). The phase change temperatures were measured with accuracy of ±0.1 °C, and the enthalpies were measured with accuracy of ±1%. Three measurements were conducted for every sample and the mean enthalpy was adopted as the latent heat, and the maximal standard deviation is no more than 2%. Thermal conductivity was measured by transient plane source technique (TPS), using a hot disk thermal constants analyzer (Hot Disk TPS 2500 S, Hot Disk AB Company, Gothenburg, Sweden). TPS was first described by Gustafsson (1991) as a technique for thermal transport studies. A resistive element is used both as heat source and temperature sensor, and is sandwiched between two specimen halves. The specimen is heated when an electrical current is applied, and the transient temperature in the sensor is recorded. Therefore, both thermal conductivity and thermal diffusivity can be evaluated from the resistance of a thin layer of an electrically conductive material inside the TPS element. The sensor/heater with a radius of 2.001 mm used in this method consists of a thin nickel foil in a double spiral pattern, which is embedded between two thin layers of Kapton polyimide protective films. In the present work, samples were pressured into tablets with a diameter of 1 cm and a thickness of 2 mm under pressure of 10 MPa using an oil pump. Measurement of thermal conductivity was carried out by putting the probe between two tablets containing the same kind of composite phase change material.

The synthesis of MOF-5 and IRMOF-3[1]

The synthesis of MOF-5 was achieved using literature procedure. $Zn(NO_3)_2 \cdot 6H_2O$ (3.41 g,11.45 mmol) and terephthalic acid H_2BDC (0.69 g,4.15 mmol) were dissolved in 100 mL of DMF. The solution was divided into 10 mL portions and transferred to 10 scintillation vials (20 mL capacity). The vials were placed in a programmable oven and heated at a rate of 2.5 °C/min from room temperature to 100 °C. The temperature was held for 18 h, and then the oven was cooled at a rate of 2.5 °C/min to the room temperature. The mother liquor from each vial was decanted, and the crystals were washed with dry DMF (3 × 12 mL) followed by one rinse with 12 mL of $CHCl_3$. The crystals were then soaked in 12 mL of $CHCl_3$ for 3 days with fresh $CHCl_3$ added every 24 h. After 3 days of soaking the crystals were stored in the last $CHCl_3$ solution.

IRMOF-3 was synthesized in the same procedure as MOF-5 except for 2-aminoterephthalic acid $H_2BDC\text{-}NH_2$ (0.75 g, 4.15 mmol) was used instead.

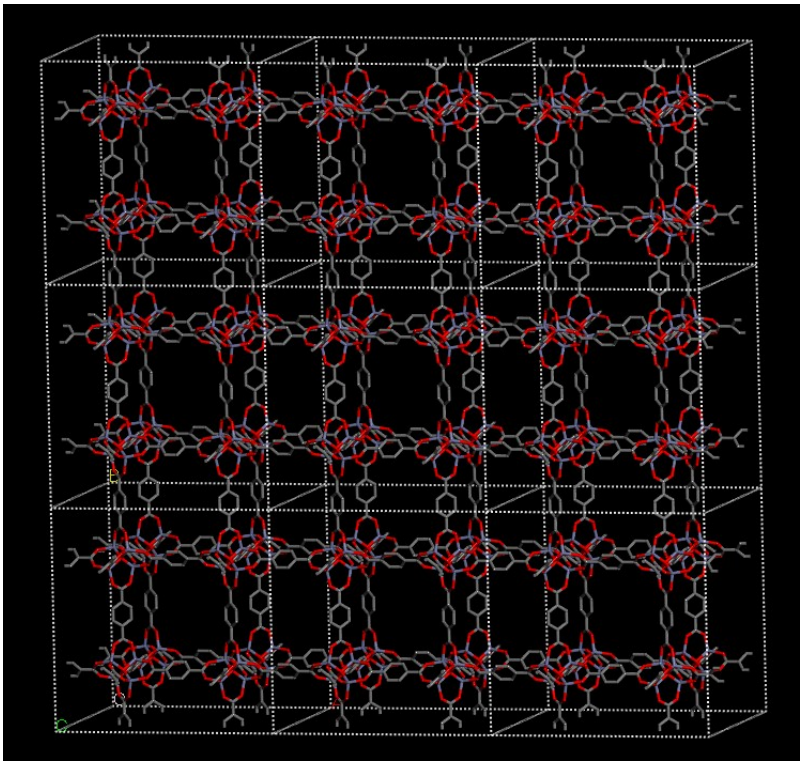

Fig. S1 Representative structure of MOF-5. The structure model was generated based on the crystal structure of MOF-5.

1

Characterizations of MOF-5 and IRMOF-3

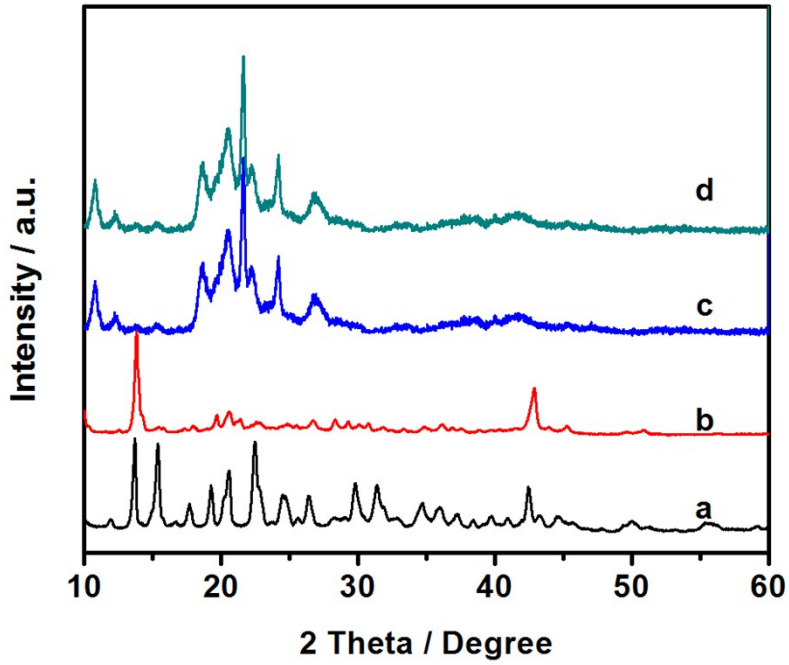

Fig S2. XRD patterns of (a) MOF-5, (b) IRMOF-3, (c) 40 wt% SA@MOF-5, (d) 60 wt% SA@IRMOF-3.

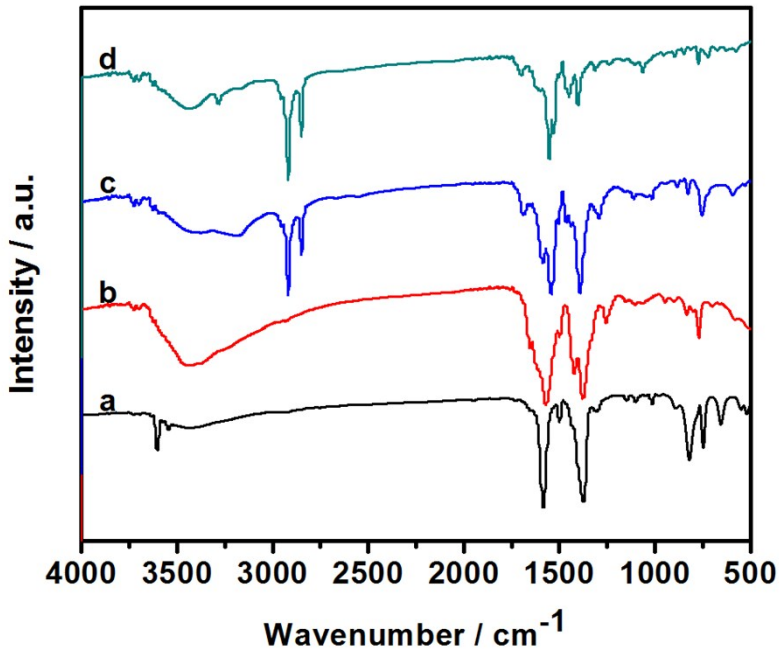

Fig S3. FTIR spectra of (a) MOF-5, (b) IRMOF-3, (c) 40 wt% SA@MOF-5, (d) 60 wt% SA@IRMOF-3.

The synthesis of UiO-66 and UiO-66-NH_2

The synthesis of MOF-5 was achieved using literature procedure. $ZrCl_4$ (0.4 g, 1.7 mmol) and acetic acid 2.85 mL(850 mmol) were added to 75 mL of N,N-dimethylformamide (DMF) and stirred until fully dissolved. Terephthalic acid (0.285 g, 1.7 mmol) was added to 25 mL of DMF and stirred until fully dissolved. The solutions were mixed in a 250 mL glass reactor vessel. The reactor was stirred at 500 RPM and held at 120 °C for 24 h. The pale yellow solid was isolated by filtration. Samples were washed three times with DMF and Methanol.

UiO-66-NH_2 was synthesized in the same procedure as UiO-66 except for 2-aminoterephthalic acid H_2BDC-NH_2 (0.311 g, 1.7 mmol) was used instead.

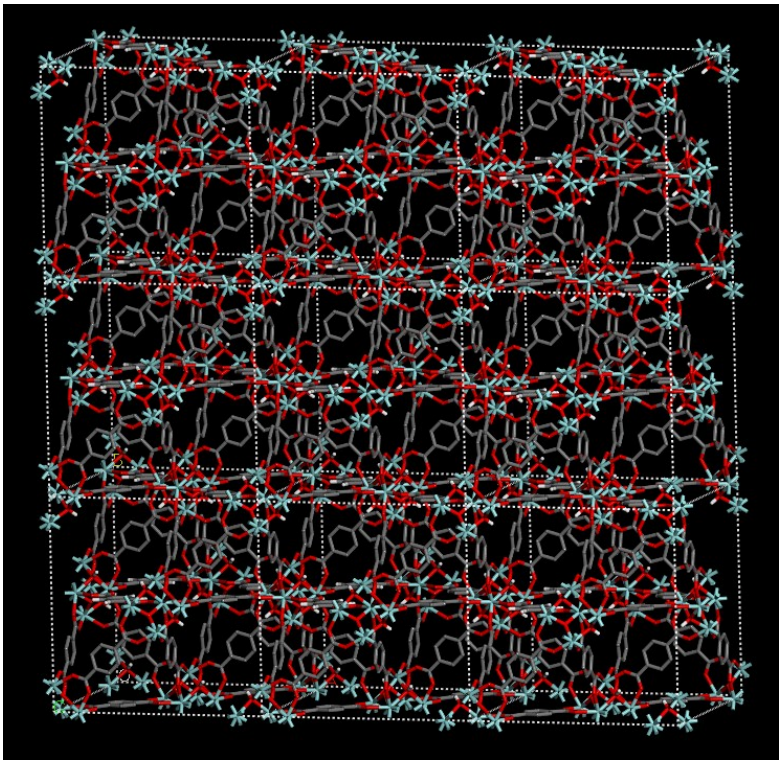

Fig. S4 Representative structure of UiO-66. The structure model was generated based on the crystal structure of UiO-66.

Characterizations of UiO-66 and UiO-66-NH_2

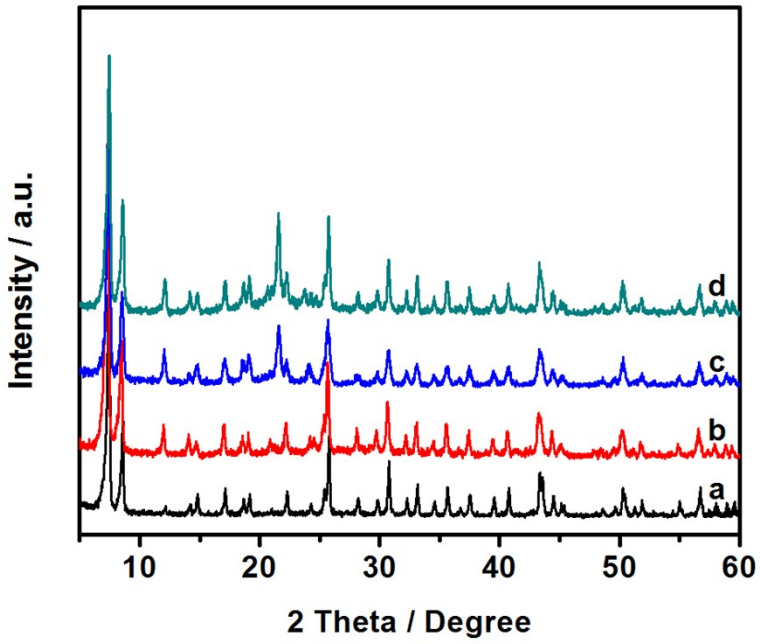

Fig. S5 XRD patterns of (a) UiO-66, (b) UiO-66-NH_2, (c) 40 wt% SA@UiO-66, (d) 50 wt% SA@UiO-66-NH_2.

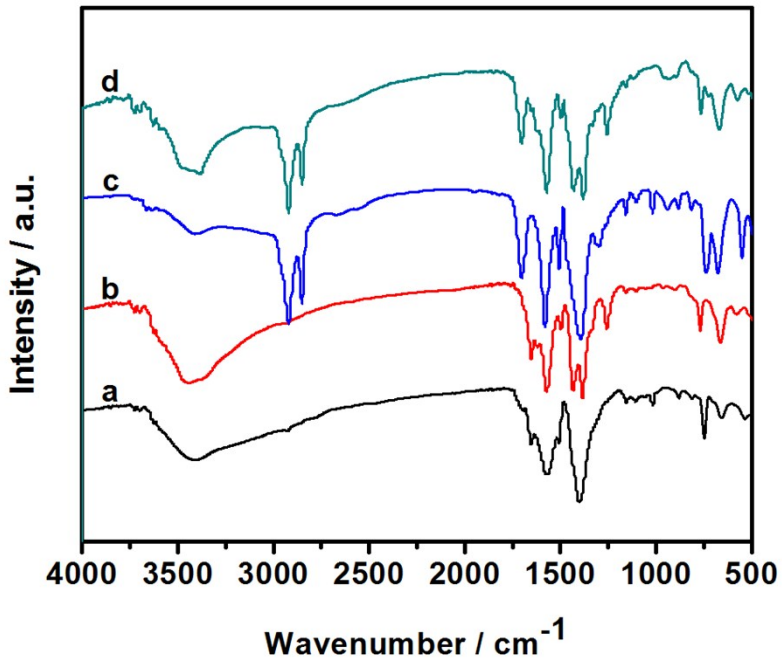

Fig. S6 FTIR spectra of (a) UiO-66, (b) UiO-66-NH_2, (c) 40 wt% SA@UiO-66, (d) 50 wt% SA@UiO-66-NH_2.

The synthesis of Al-MIL-53 and Al-MIL-53-NH_2

Al-MIL-53 was synthesized under the hydrothermal condition. $Al(NO3)_3 \cdot 9H_2O$ (0.787 g, 2.1 mmol), terephthalic acid (H_2BDC, 0.533 g, 3.21 mmol) and 0.64 g F127 were mixed with 50 mL of N,N-dimethylformamide (DMF) stirred until fully dissolved. Let the solution set still at 120 °C for 36 h .After cooling down, The solid was isolated by filtration. Samples were washed three times with DMF and Methanol.

Al-MIL-53-NH_2 was synthesized in the same procedure as Al-MIL-53 except for 2-aminoterephthalic acid H_2BDC-NH_2 (0. 575 g, 3.21 mmol) was used instead.

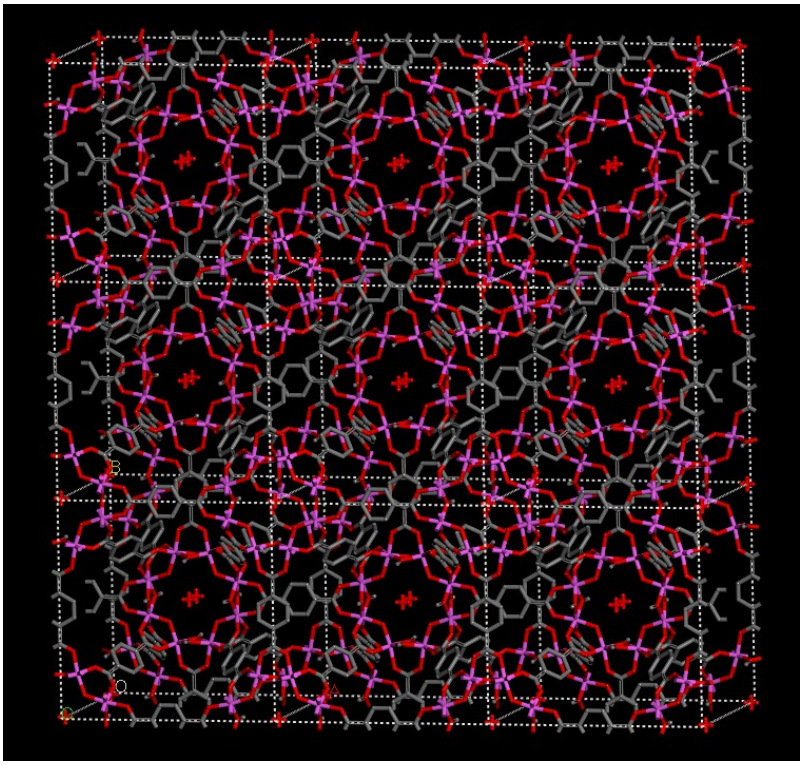

Fig. S7 Representative structure of Al-MIL-53. The structure model was generated based on the crystal structure of Al-MIL-53.

Characterizations of Al-MIL-53 and Al-MIL-53-NH_2

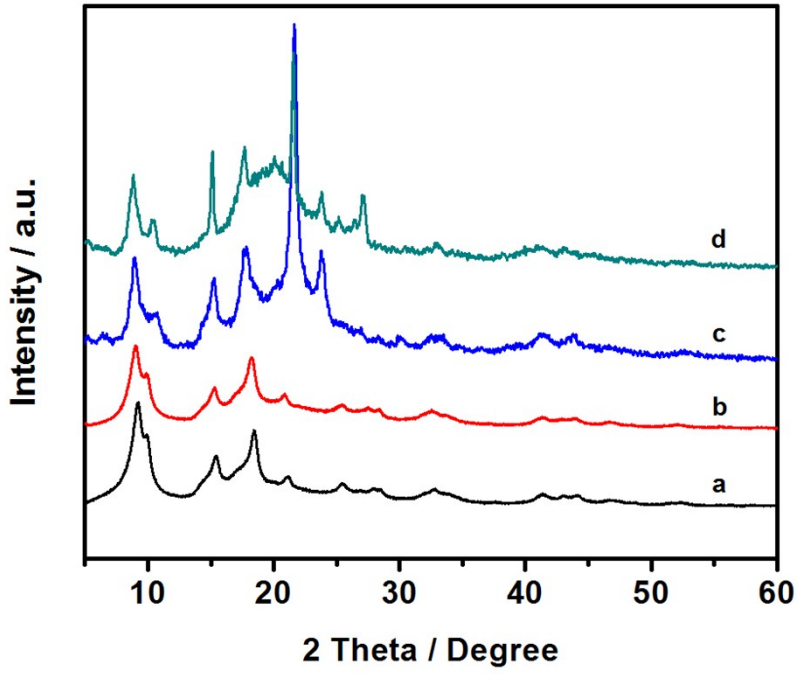

Fig. S8 XRD patterns of (a) Al-MIL-53, (b) Al-MIL-53-NH_2, (c) 40% SA@Al-MIL-53, (d) 50% SA@Al-MIL-53-NH_2.

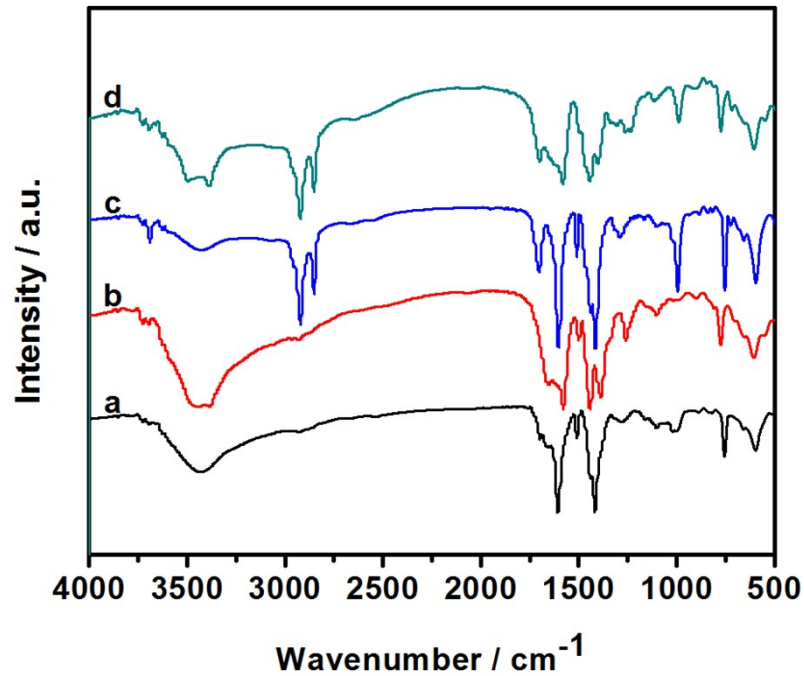

Fig. S9 FTIR spectra of (a) Al-MIL-53, (b) Al-MIL-53-NH_2, (c) 40% SA@Al-MIL-53, (d) 50% SA@Al-MIL-53-NH_2.

The synthesis of Cr-MIL-101 and Cr-MIL-101-NH_2[2]

The synthesis of Cr-MIL-101 was achieved under the hydrothermal reaction using H_2BDC (1.66 g, 8.0 mmol) with $Cr(NO_3)_3.9H_2O$ (4.0 g, 8.0 mmol), fluorhydric acid (2 ml) and H_2O (48 ml). The solution mixed was heated 220 ºC to for 8 hours.

The synthesis of Cr-MIL-101-NH_2 was achieved using one-step procedure of the literature report. In a typical experiment, H_2BDC-NH_2 (3.2 g, 8.0 mmol) and $Cr(NO_3)_3 \cdot 9H_2O$ (3.2 g, 8.0 mmol) NaOH (0.8 g, 20 mmol) were added to 60 mL water. The resulting suspension was stirred for 30 min at room temperature then heated under autogeneous pressure at 150 °C for 12 h in a Teflon-lined autoclave. After cooling to room temperature, the solid product was isolated as a green powder by centrifugation and washed three times with DMF and Methanol.

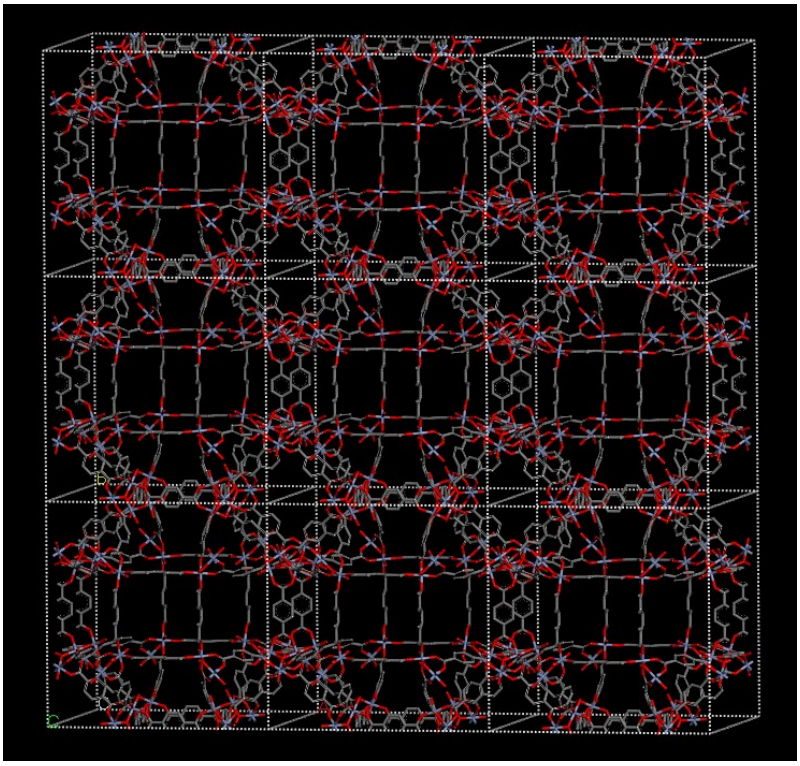

Fig. S10 Representative structure of Cr-MIL-101. The structure model was generated based on the crystal structure of Cr-MIL-101.

[2] G. Férey, C. Mellot-Draznieks, C. Serre, F. Millange, J. Dutour, S. Surblé and I. Margiolaki, Science, 2005, 309, 2040-2042

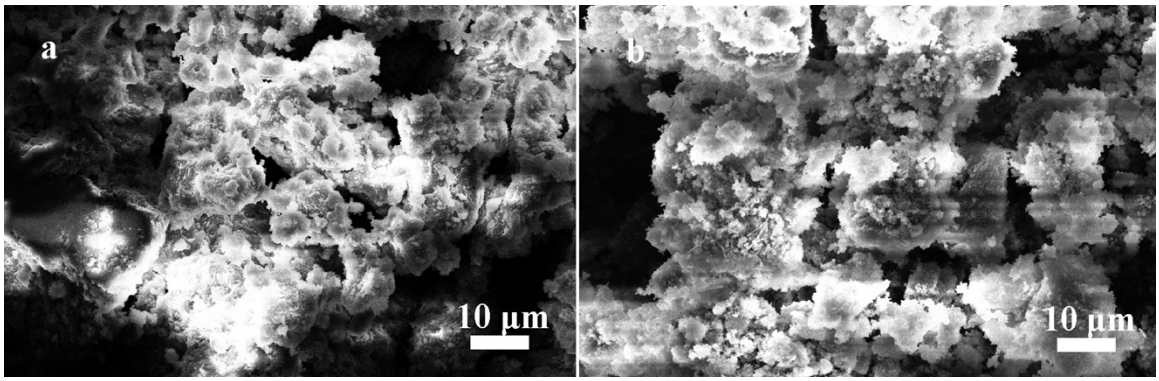

Fig. S11 SEM images of (a) 50 wt% SA@Cr-MIL-101-NH_2 and (b) 60 wt% SA@Cr-MIL-101-NH_2.

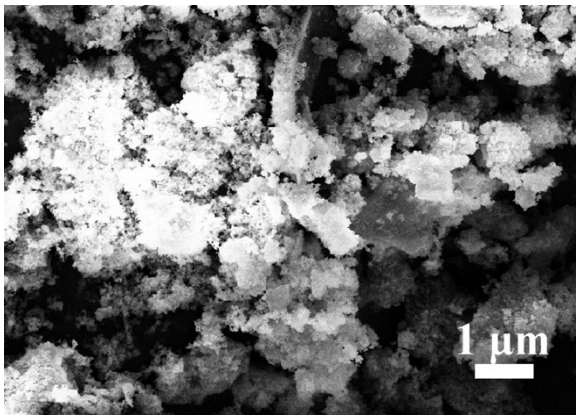

Fig. S12 SEM of 80% SA@Cr-MIL-101-NH_2.

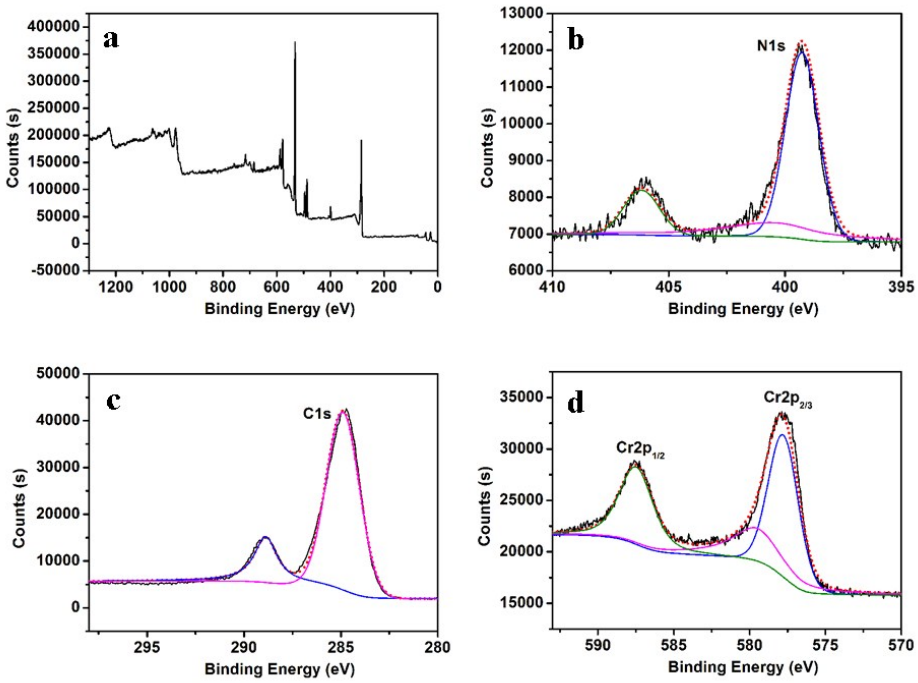

Fig. S13 XPS of Cr-MIL-101-NH_2 matrix.

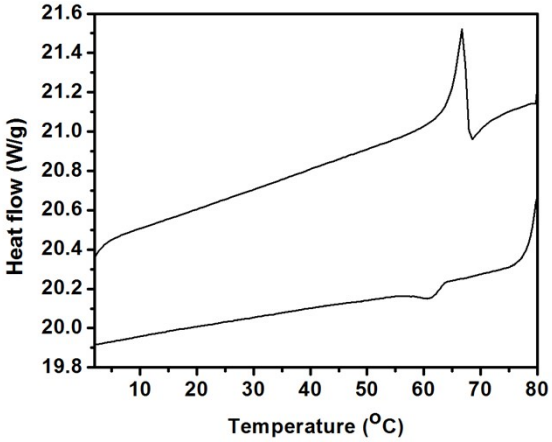

40 wt% SA@MOF-5

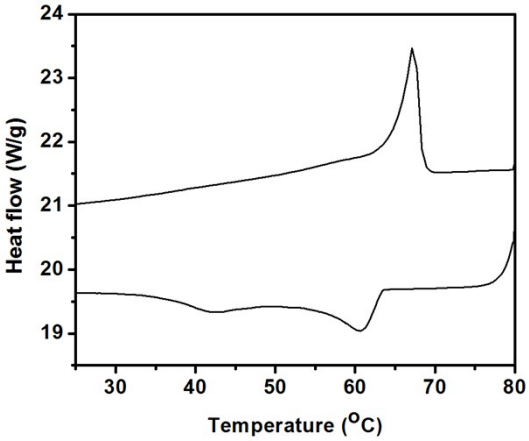

60 wt% SA@IRMOF-3

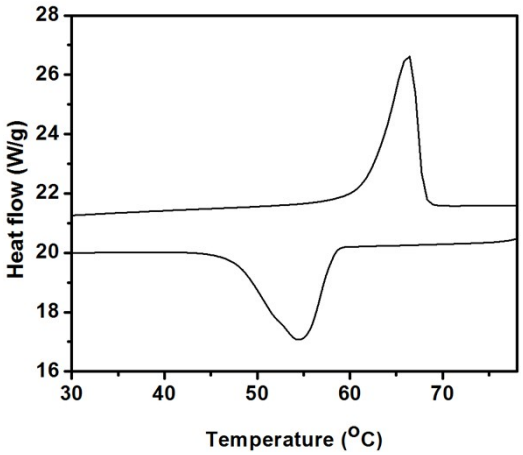

40 wt% SA@UiO-66

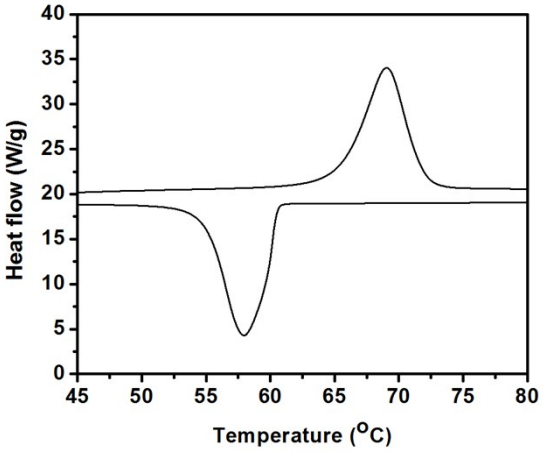

50 wt% SA@UiO-66-NH_2

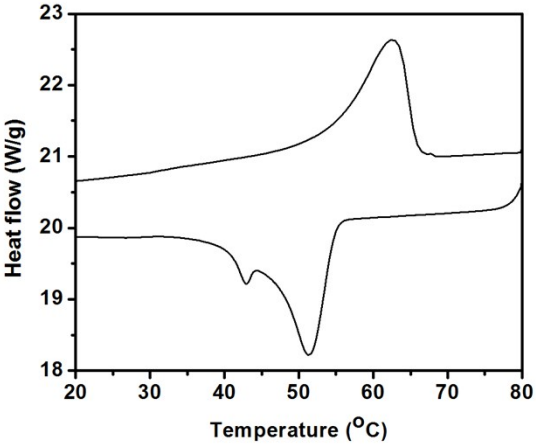

40 wt% SA@Al-MIL-53

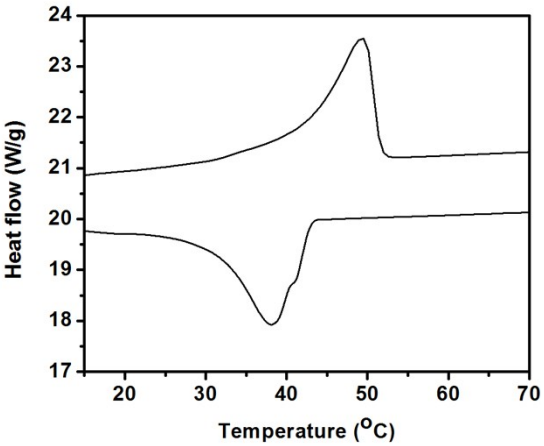

50 wt% SA@Al-MIL-53-NH_2

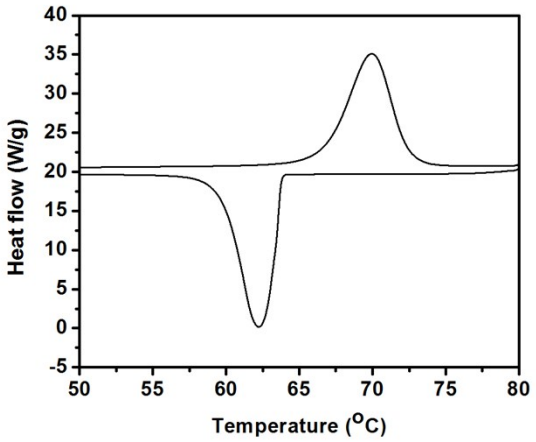

40 wt% SA@Cr-MIL-101

Fig. S14 The thermal properties of various loading of SA@MOF matrix.

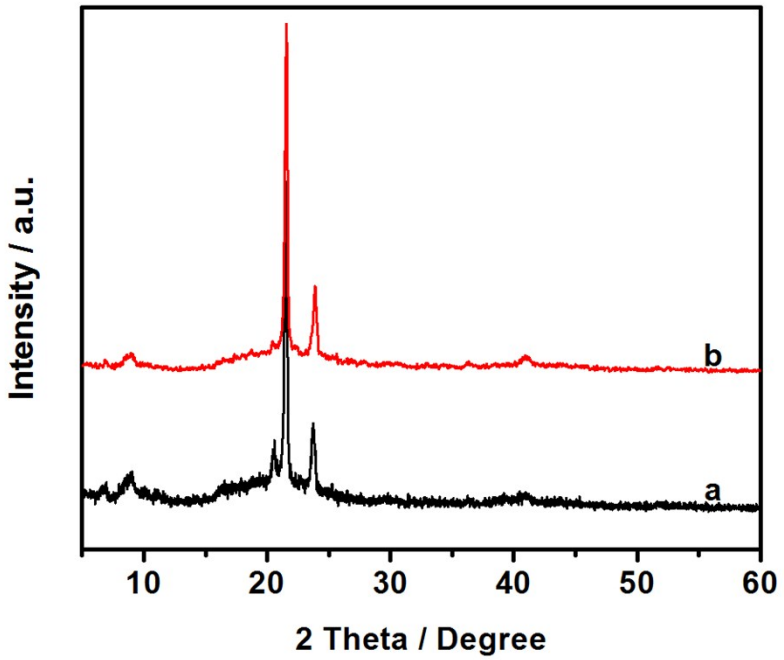

Fig. S15 PXRD of 70% SA@Cr-MIL-101-NH_2 before and after 50 times thermal cycling, a) before cycling, b) after cycling.

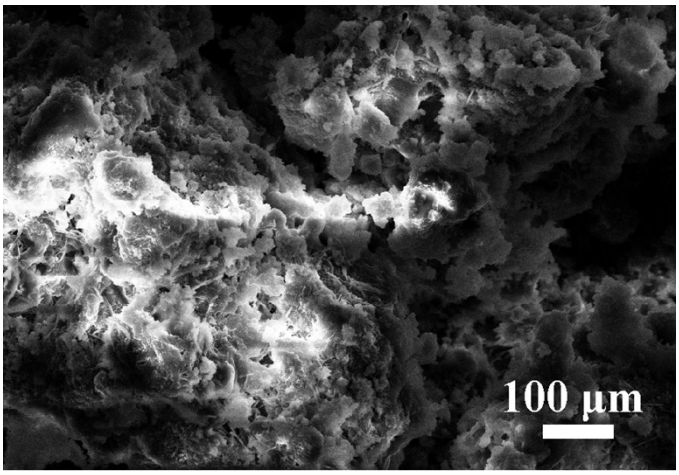

Fig. S16 SEM of 70% SA@Cr-MIL-101-NH_2 after 50 times thermal cycling

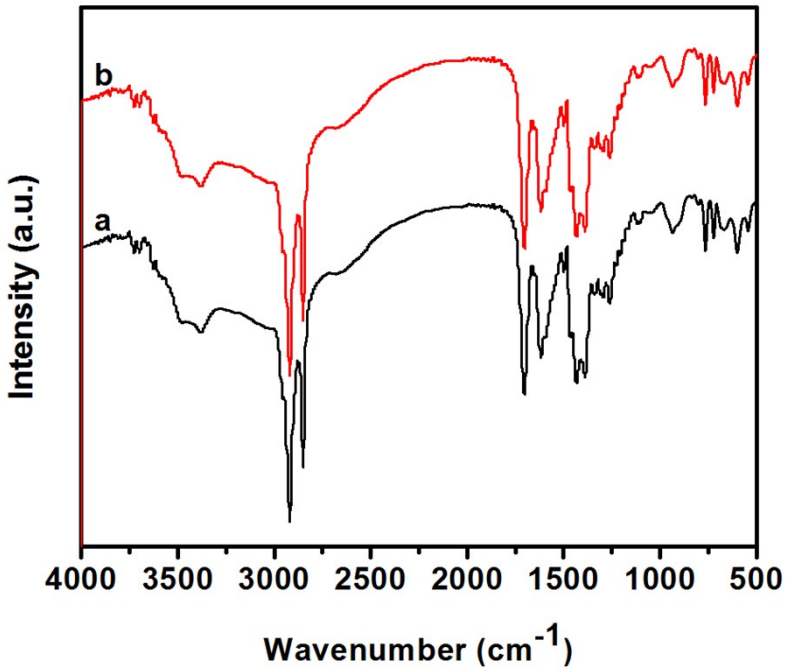

Fig. S17 FTIR of 70% SA@Cr-MIL-101-NH_2 before and after 50 times thermal cycling, a) before, b) after.

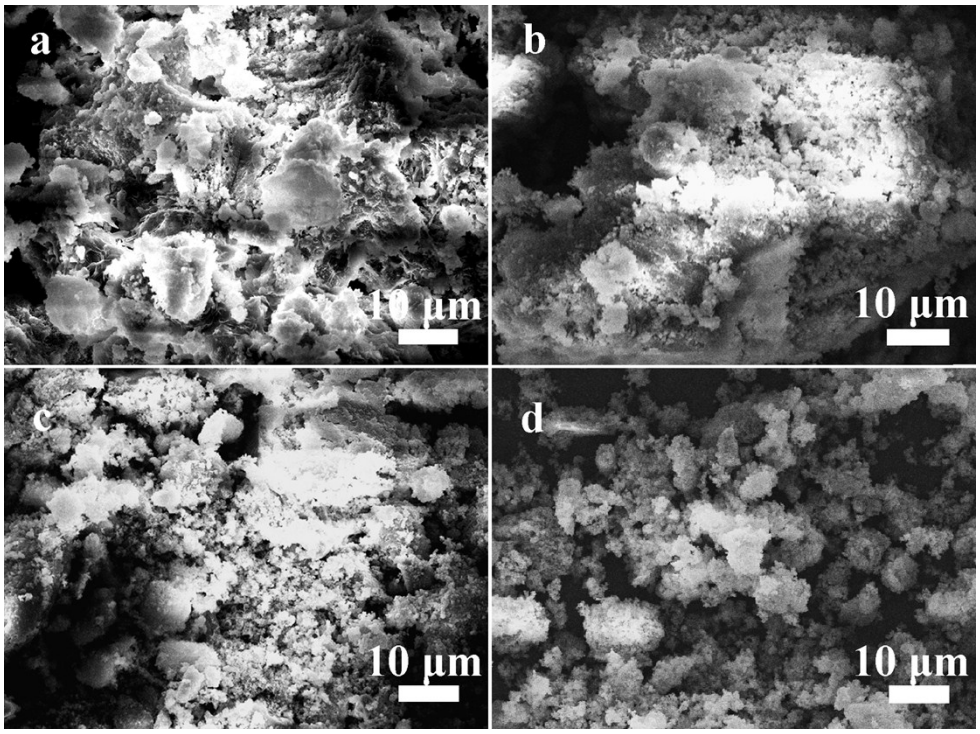

Fig. S18 SEM images of various organic acid and Cr-MIL-101-NH_2 supports. (a) Palmitic acid@Cr-MIL-101-NH_2, (b) Myristic acid@Cr-MIL-101-NH_2, (c) Lauric acid@Cr-MIL-101-NH_2, (d) PEG-2000@Cr-MIL-101-NH_2.

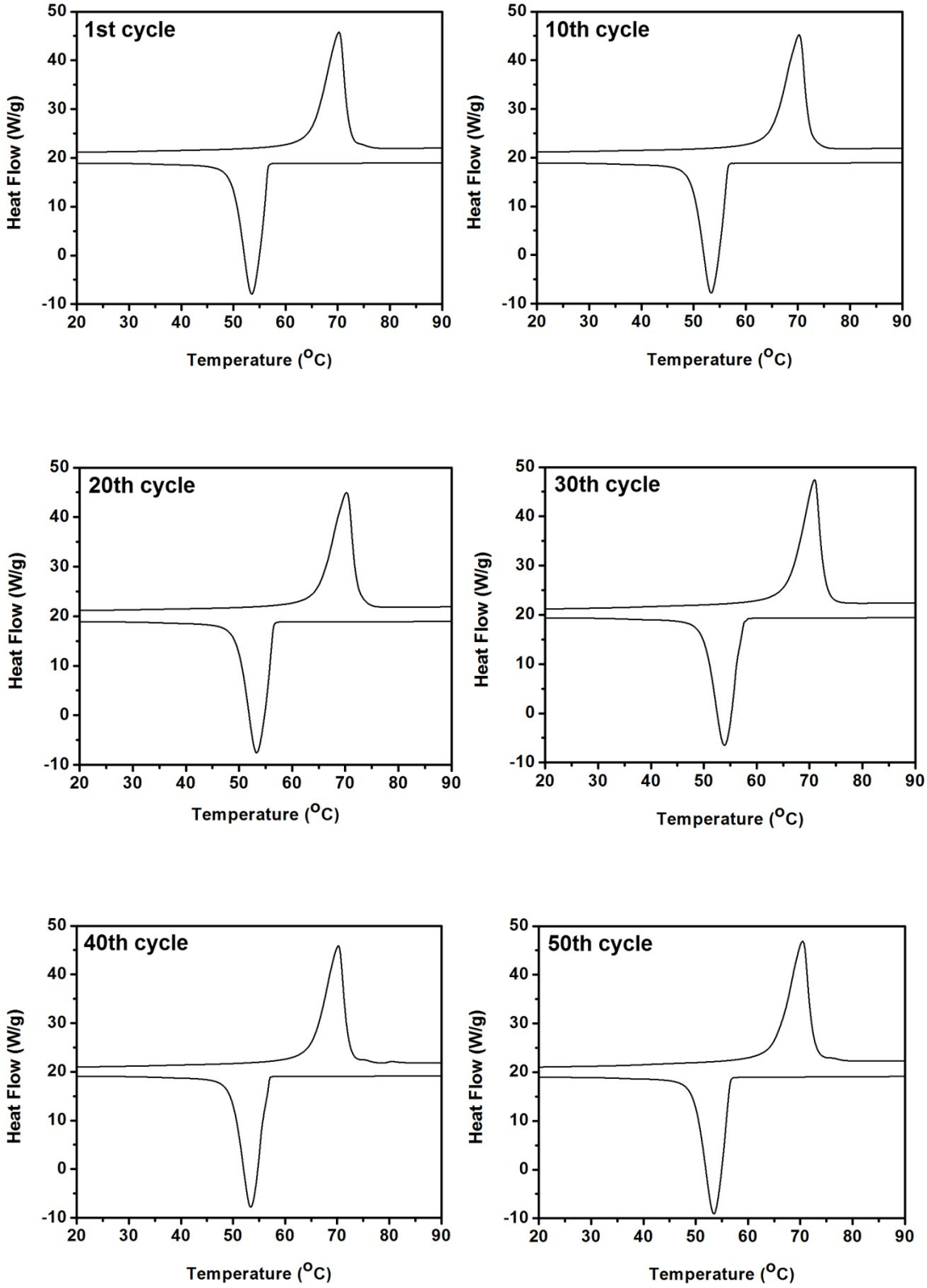

Fig. 19 50 times thermal recycling of 70 wt% SA@Cr-MIL-101-NH_2

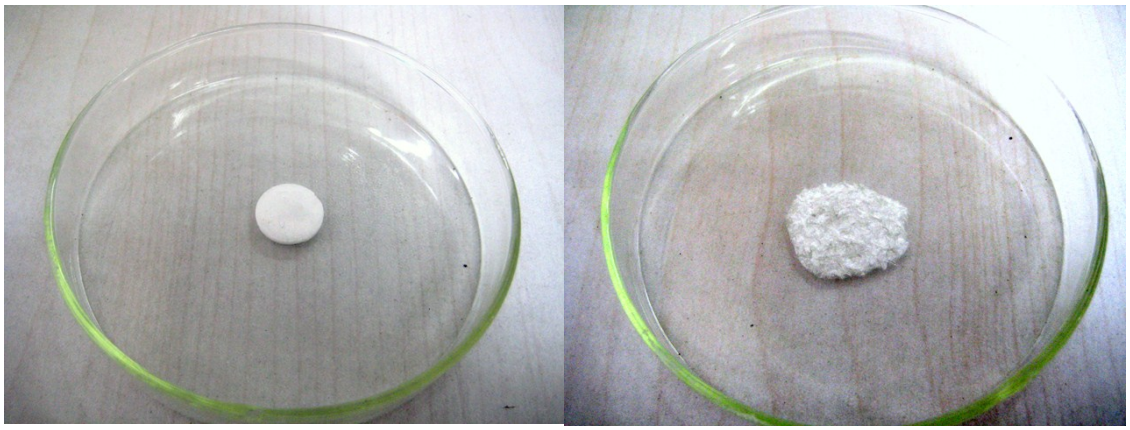

Fig. S20 Digital photographs of pure stearic acid (left), after one thermal cycle at 80 ºC (right).

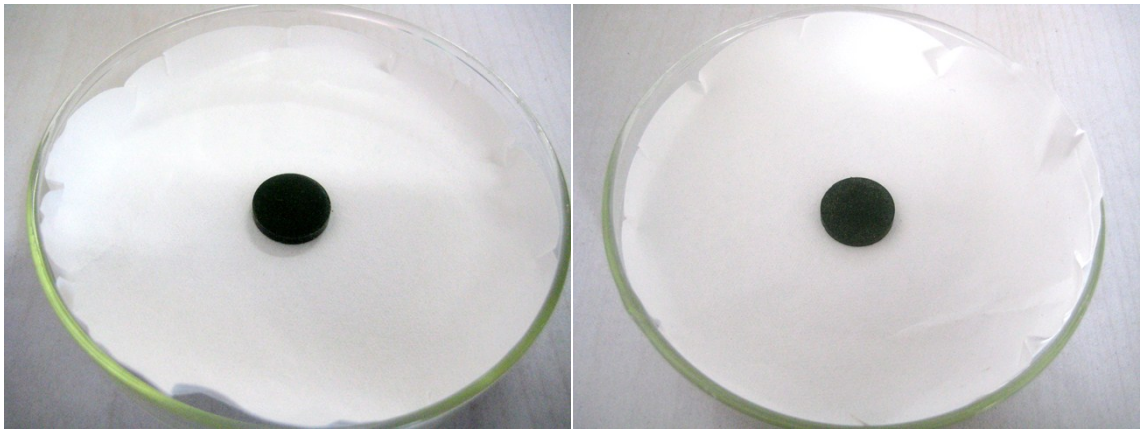

Fig. S21 Digital photographs of SA@Cr-MIL-101-NH_2 (left), b) after one thermal cycle at 80 ºC (right).

Table S1. Maximum PCM incorporation capacity of stearic acid on various PCM matrix.

Entry	Fatty acid @Matrix	BET surface area (m^2/g) and pore size of the matrix	Max. mass percentage (wt%)	ΔH_m (J/g)	ΔH_f (J/g)	Ref.
1	Lauric acid /expanded perlite	1.35/~ 2μm	60	93.4	94.8	1
2	Stearic acid/activated montmorillonite	Not available	47.5	84.4	88.5	2
3	Capric–myristic acid /expanded perlite	1.35/~ 2μm	55	85.40	89.75	3
4	Capric acid/halloysite nanotube/graphite	57.76/2-6 nm	60	75.40	75.35	4
5	SA/GB	71.18/9 nm	36.3	50.93	49.98	5
6	SA/GBm	130.34/13 nm	45.5	84.64	84.14	5
7	SA/Expanded graphite	Not available	50	90.36	88.83	6
8	SA/Porous carbon	Not available	75	90.45	87.76	7
9	**SA/Cr-MIL-101-NH_2**	**1998/1.2-1.5 nm**	**70**	**120.53**	**117.59**	**This work**

1. A. Sarı, A. Karaipekli and C. Alkan, *Chem. Eng. J.*, 2009, **155**, 899.
2. Y. Wang, H. Zheng, H. X. Feng and D. Y. Zhang, *Energy Build.*, 2012, **47**, 467.
3. A. Karaipekli and A. Sari, *Renew. Energy*, 2008, **33**, 2599.
5. C. Li, L. Fu, J. Ouyang and H. Yang, *Sci. Rep.*, 2013, **3**, 1908. 4. D. Mei, B. Zhang, R. Liu, Y. Zhang and J. Liu, *Sol. Energy Mater. Sol. Cells*, 2011, **95**, 2772.
6. G. Y. Fang, H. Li, Z. Chen, X. Liu, Energy, 2010, **35**, 4622.
7. N. Wu, X. W. Wu, C. Q. Shi, J. Ji, W. Liu, Journal of Thermophysics and Heat Transfer, 2016, **30**, 192.